

Journal of Materials Chemistry A

Accepted Manuscript



This is an *Accepted Manuscript*, which has been through the Royal Society of Chemistry peer review process and has been accepted for publication.

Accepted Manuscripts are published online shortly after acceptance, before technical editing, formatting and proof reading. Using this free service, authors can make their results available to the community, in citable form, before we publish the edited article. We will replace this *Accepted Manuscript* with the edited and formatted *Advance Article* as soon as it is available.

You can find more information about *Accepted Manuscripts* in the [Information for Authors](#).

Please note that technical editing may introduce minor changes to the text and/or graphics, which may alter content. The journal's standard [Terms & Conditions](#) and the [Ethical guidelines](#) still apply. In no event shall the Royal Society of Chemistry be held responsible for any errors or omissions in this *Accepted Manuscript* or any consequences arising from the use of any information it contains.

Cite this: DOI: 10.1039/c0xx00000x

www.rsc.org/xxxxxx

ARTICLETYPE

Atmospheric growth and strong visible luminescence of anatase titanium oxide films with various orientations

M. L. Li,^{a,b} G. S. Huang,^{b*} J. Zhang,^a J. J. Shi^{a*} and Y. F. Mei^b*Received (in XXX, XXX) Xth XXXXXXXXXX 20XX, Accepted Xth XXXXXXXXXX 20XX*

DOI: 10.1039/b000000x

In atmospheric pressure, anatase TiO₂ films with various nano-morphologies have been grown on quartz substrate by non-thermal TiCl₄/O₂/Ar reactive plasma vapor deposition. High concentration of oxygen vacancies and undercoordinated Ti atoms are incorporated into the crystal lattice of the deposited films, which can be tuned by changing the discharge conditions such as temperature and vapor flow rate. Strong visible luminescence is disclosed in the deposited film and originates from the radiative recombination of trapped electrons due to uncoordinated Ti atoms and oxygen vacancy. To clarify growth mechanism, an analytical model is proposed to explain the corresponding discharging process. And we find the theoretical predictions agree well with experimental results. By effectively adjusting the morphology and lattice crystallinity, we believe this work can provide an expedient and controllable way to fabricate anatase films with interesting optical properties, which can meet the demands for complex practical situations to the maximum degree.

Introduction

Titanium dioxide (TiO₂) is an industrially important wide-band gap semiconductor with plenty of applications in a wide range of technological fields such as heterogeneous catalysis, photo-electrolysis, bio-compatibility, and sanitary disinfection,¹⁻⁵ which have spurred a great deal of researches to focus on its bulk structures and surface properties. Owing to the advantages of some special facets in TiO₂, which is related to their unique lattice properties and widely applied to the fields like the photocatalytic process,^{6,7} it is believed that there is great necessity to emphasize the importance of TiO₂ nanostructures fabricated with certain crystal structure. For instance, anatase TiO₂ exhibits a higher activity than other polymorphs and has been generally used for renewable energy development and biomedical areas.^{8,9}

The {101} facets of anatase TiO₂ has always attracted attention because it is favorable to most of the practical situations mainly due to its thermodynamically stability. As predicted by the Wulff [10], the most stable form of the anatase polymorph is a tetragonal bipyramidal structure in which {101} facets are primarily exposed (more than 94 %), with a small percentage of {001} facets. On the other hand, anatase {001} facet is also found to be beneficial since the crystal with these surfaces exhibits high carrier mobility, low incident light reflection loss, and large reactive surfaces.^{11,12} However, the highly reactive facets can hardly survive in complex situations and will diminish rapidly during the crystal growth due to the minimization of surface energy.¹³

Much attention has been also paid to tune the lattice structure so far to minimize the energy loss of the high-energy {001} facet, among which the fluorine involved methods are mentioned frequently.^{14,15} According to the recent results of Yang et al.,¹⁶ the introduction of hydrofluoric acid (HF) during the hydro-thermal synthesis of TiO₂ can stabilize the {001} facet, allowing for the formation of truncated bipyramidal structures in the micrometer-size range. Nevertheless, such method can only enhance the percentage of {001} facets to 47 % and has met with a lot of difficulties in further improvement. Other attempts such as plasma-assisted molecular beam epitaxy, ion implantation, and electron bombardment, which are expected to induce the formation of anatase {101} and {001} facets, however, suffered from the annihilation of the high energy surface and the lattice disorder led by the constant disturbance of newly formed oxygen vacancies (OVs).¹⁷⁻²⁰ Furthermore, it has been reported that specific lattice defects are selectively introduced into TiO₂ structure for applications like photocatalysis, photoconversion and gas sensor as well.²¹⁻²³ For example, Ti³⁺ can help to form a microstructured composite between hydrophilic and oleophilic phases, which will finally enhance the photoconvertible surface wettability.²⁴ Wang et al. reported the effect of OV's and hydrogen treatment help increases the donor density of TiO₂ nanowires by 3 orders of magnitudes and finally enhance the photocurrent TiO₂ under UV exposure.²⁵ Therefore, it is challenge to produce TiO₂ structure with designed lattice orientation and demanded defects so as to meet the requirement of various applications.

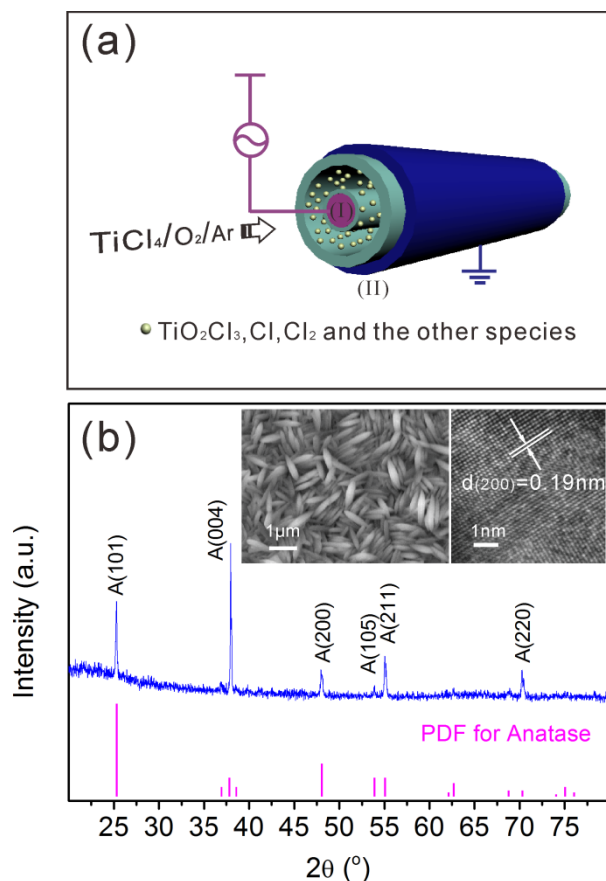


Fig. 1. (a) Schematic representation of the fabrication process of the anatase TiO₂ film; (b) A typical XRD pattern of the fabricated sample. A: anatase. The left and right insets show corresponding SEM and HRTEM images respectively.

In this work, anatase TiO₂ film with controllable orientation along (101) or (001) can be fabricated by an atmospheric discharge process without any catalysts or templates engaged. Strong emission can be seen in the photoluminescence measurement when the deposited film is excited by laser, which can be mostly ascribed to the effect of OV_s and uncoordinated Ti atoms. The experimental results demonstrate a complex growing process, and we found that the lattice structure of the anatase TiO₂ can be altered by changing reaction temperature and the precursors' concentrations. The method used in this work is compatible to the mass production in industrial manufacturing, and therefore can be widely adopted in the future.

Experimental

Atmospheric pressure non-thermal reactive plasma of TiCl₄/O₂/Ar mixture was applied to produce TiO₂ film. The PECVD process was taken place in a home-made atmospheric pressure plasma reactor composed of two coaxial quartz tubes with a gap of 1.5 mm. A 13.56 MHz radio-frequency power supply was applied to ignite the plasma in the space between the two electrodes (I) and (II), as shown in Fig. 1(a). TiCl₄/O₂/Ar mixture was fed into the reactor through mass flow controllers and the anatase TiO₂ film was obtained directly on the quartz substrate placed in the chamber after 1-2 h without any post-

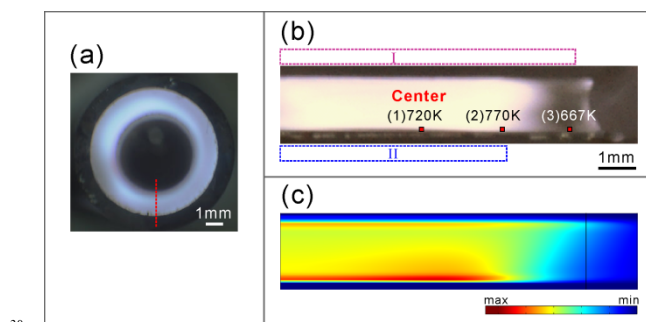


Fig. 2. (a) Photograph of the plasma reactor during the discharge process (cross-section view perpendicular to the axis). (b) Photograph of the lateral view of the plasma reactor during the discharge process: (1) The in-glow discharge zone, (2) The boundary zone, (3) The afterglow discharge zone. The lateral view of the reactor in (b) corresponds to the red dashed line in (a). (c) Simulated electron density in the reactor. The geometry is same to that in (b).

treatments. During the discharging process, the temperature of the reactor was monitored by thermocouples. The morphology and crystal structure of the deposited film was examined using field emission scanning electron microscopy (FE-SEM, S-4800, Hitachi), transmission electron microscopy (TEM, JEM-2010, JEOL), and X-ray diffraction spectrum (XRD, D/max-2550 PC, RIGAKU). X-Ray photoelectron spectrometer (XPS, PHI 5000C ESCA) was involved to examine the lattice defects in the film. A 325 nm He-Cd laser with pump power of 30 mW was used as excitation source to measure the PL spectra of the samples in order to investigate the optical properties.

Results and discussion

Fig. 1(a) is a schematic representation illustrating the deposition process. A quartz substrate was placed into the reactor to collect the TiO₂ film formed close to the cathode. The introduced reactive plasma of TiCl₄/O₂/Ar gradually spread into the whole atmosphere and was then decomposed into various species including TiO₂Cl₃, O₂, O, Cl, Cl₂, and ClO, which are all contributed to the formation of TiO₂ through overall reaction:



From a typical SEM image shown in the left inset of Fig. 1(b), one can see the sample is a film consisting of uniform small grains in diamond shape with large aspect ratio. To check the crystal structure of the sample deposited on substrate, we carried out XRD measurement and the results are shown in Fig. 1(b), and all the direction peaks in the XRD pattern can be well indexed to anatase TiO₂ (see the peak positions from standard PDF database). Importantly, the relative intensities of the diffraction peaks obviously suggest a partially preferential growth direction of TiO₂ sample along (004) direction. The HRTEM characterization also demonstrated clear lattice fringes with distance of 0.19 nm (from (200) lattice plane of anatase TiO₂), as shown in the right inset of Fig. 1. The HRTEM image further confirms the formation of anatase phase with good crystal quality.

It is natural to know that the distribution of plasma inside the chamber cannot be completely uniform. This was proven

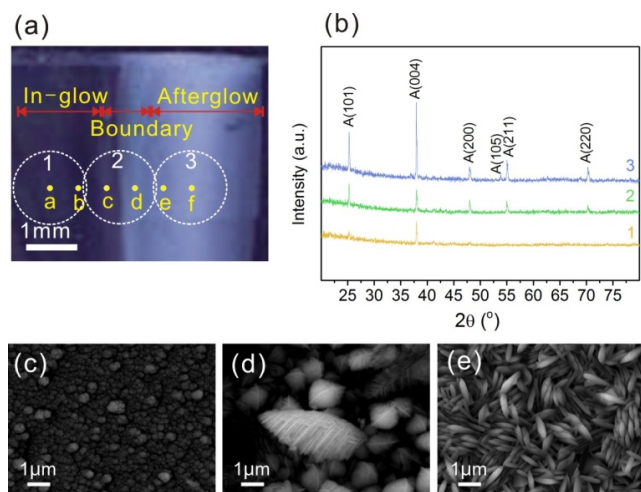


Fig. 3. (a) A photograph of TiO₂ film fabricated by PECVD process. Film in in-glow, boundary, and afterglow zones are labelled. Samples from three testing spots were selected for further characterization: spot 1 is located in the in-glow zone, spot 2 is in the boundary zone, and spot 3 is in the afterglow discharge zone. (b) XRD patterns of samples taken from the three test points marked in (a). A: anatase; (c)-(e) The corresponding SEM images of the samples from the three test spots (1-3) mentioned in (a).

by normal photography of the discharge glow in the plasma reactor. Fig. 2(a) shows a photo of the cross-section view of the reactor during plasma discharge. The glow between the two quartz tubes is brilliant and almost homogeneous due to the central symmetry. However, the photo of the lateral view of the reactor (Fig. 2(b)) shows the glow is not uniform along the reactor axis: the glow in the middle part is much brighter than that near the edge. A deep analysis was carried out with the help of theoretical simulation. Fig. 2(c) shows the corresponding simulated electron density during plasma discharge (lateral view corresponds to (b)). The simulated results agree well with the experimental results and on the basis of the electron density (glow intensity) distribution, the chamber can be roughly divided into three regions: (1) The in-glow discharge zone is depicted as the section at the center of the reactor and suffers from the most severe plasma attacking; (2) The boundary area describes the area around the edge of the cathode where the ions is not so crowded as in the in-glow discharge zone; (3) The afterglow zone is the part which is not besieged by main ion flow and locate in the end of the apparatus. Obviously, the ions are mostly collected in the in-glow discharge zone in which a bright light is emitted. The temperatures of different regions during the discharge have also been obtained as evidence of the successive change happened in the reactor. It is detected that although no exterior heating device was used, the boundary section reached the highest temperature (770 K) by a self-heating process and temperatures of the in-glow discharge and the afterglow discharge zones are only 720 and 667 K, respectively. The difference in plasma intensity and temperature, which originate from radio-frequency power supply and corresponding electromagnetic field, should significantly influence the film deposition and thus needs to be carefully investigated. The substrate as well as the sample in the in-glow section experience more ion attacks while the

substrate/sample locates in afterglow section only suffers from slight collision

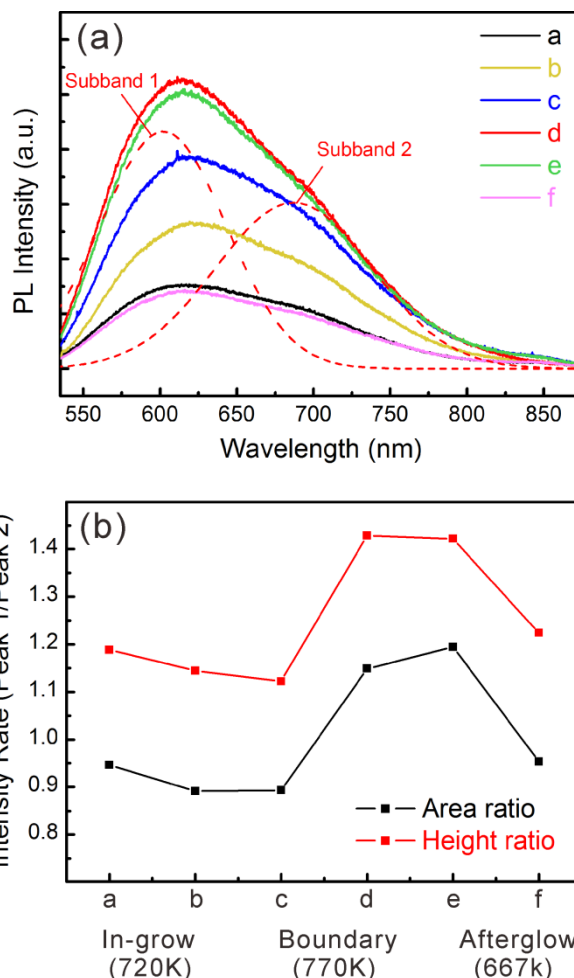


Fig. 4. (a) PL spectra from the as-prepared TiO₂ film corresponding to testing orientation of the test spots marked in Fig. 2(a). The dashed lines are the fitting curves (two Gaussian subbands) for the spectrum from spot 4. (b) Integral area and height ratios of the two subbands at 6 testing spots (a-f).

and such difference should produce TiO₂ structures with different morphological features, which will be detailedly discussed in the following sections.

A quartz substrate was placed into the chamber which runs through all of the three zones and therefore is able to obtain the entire information of samples formed at different regions in one deposition. A photograph of the substrate with samples deposited is displayed in Fig. 3(a). The difference of film formed is noticeable even by naked eye. The TiO₂ which grew in moderate atmosphere (the after-glow zone) have formed a thick film, while in the region with intense ion attack (the in-glow zone) one can only see a very thin film. Here, to probe the difference more specifically, we took 3 typical samples from in-glow zone, boundary zone, and after-glow zone respectively (see spots 1, 2, and 3 in Fig. 3(a)). Typical SEM images of these 3 samples are shown in Figs. 3(c), 3(d), and 3(e), respectively. We found that the largest crystal grains are formed in the boundary zone where the highest temperature was achieved (see also Fig. 2). This results accords with previous literature in which high temperature

is confirmed to be beneficial for the crystal growth.²⁶ The kinetic process of crystal growth suggests that the higher the intermediate primary precursor density and the temperature, the higher the crystal growth rate and the higher the crystal lattice regularity.²⁷ Thus the anatase crystal grown in boundary zone is confirmed to be large but less uniform. When it comes to the after-glow discharge zone, grains became smaller because the concentration of plasma drops dramatically in this place. On the other hand, even smaller crystals are observed in the in-glow zone (spot 1). The phenomenon is not hard to understand, since there is no time for plasma to form a big crystal grains before the ions in in-glow zone destroy it. In addition to the morphology evolution, the structural properties of the samples are also different. In order to probe the structural properties of the samples, XRD patterns of the three spots were collected and are exhibited in Fig. 3(b). All of the diffraction peaks shown prove the existence of only anatase TiO₂ in the 3 samples. In general, diffraction peaks are weak in sample from spot 1 (in-glow zone) and are much stronger in sample from spot 3 (after-glow zone), probably due to the larger thickness of the film at spot 3. However, some specific diffraction peaks appear to be more obvious than others in certain sample. Anatase (101) and (004) peaks are the two dominate peaks shown in the patterns and therefore chosen for further discussion. Careful comparison has been made and we discover that both of the integral area and the height ratio of these two peaks in different samples experience visible fluctuation. In the samples from in-glow and the after-glow discharge zones, (004) peak owns higher intensity than (101) peak, while they possess similar intensities in the sample from the boundary zone. The difference in the intensities of the XRD peaks, i.e. the different crystal structures, should be mainly due to the variant temperatures in plasma discharge. The increased temperature in the boundary zone largely activated the ions and the film finally tends to form the stable facet with lower surface energy.²⁸

PL spectroscopy as a highly sensitive technique to detect the structural properties in TiO₂ crystal,²⁹ herein we tried to study the structure of the TiO₂ films in more details by investigating their light emission properties. To achieve this, we selected 6 small spots (spots a-f, diameter: ~2 μm) between the spots 1 and 3 in Fig. 3(a) with equal steps and measured corresponding PL spectra. The broad PL peaks clearly demonstrate that luminescent defects exist in the TiO₂ films fabricated by current PECVD process.²³ We notice that the intensities of both the PL subbands firstly increase from the in-glow discharge zone towards the boundary line, and then reduce at the after-glow zone. This phenomenon should be related to the plasma distribution and the system temperature as well. The boundary zone owned the highest discharge temperature and was surrounded with a higher ion concentration, which finally leads to the thickest film and more opportunities for various lattice defects in the growth process. On the other hand, due to the excessive ion collisions, the film formed in the in-glow zone is too thin to emit intense light. Moreover, the obviously asymmetrical feature of the PL peaks suggests that more than one PL center should contribute to the broad band.³⁰ To clarify the origin of the broad band, each PL band is divided into two

Gaussian subbands. A typical fitting result of spectrum d is shown in dashed lines in Fig. 4(a). The fitting results of all the spectra illuminate that the two subbands are located at ~600 and ~680 nm, respectively. The integral area and the height of the subbands were recorded and their ratios between the two subbands were calculated and the results are plotted in Fig. 4(b). One can see that the ratios reach the maximum at spots d and e indicating the subband at shorter wavelength (subband 1) suffered from a visible inferior in the boundary zone.

It has been referred in the previous work that trapped holes like OVs tend to form on anatase nanoparticle, which will eventually lead visible emission at the wavelength of around 600 nm.^{23,31,32} In present PECVD process, the precursor species aggregated into (TiO_xCl_y)_n nanoparticulates and fast nucleate into loosely-packed web-like nanosized anatase nuclei.³³ In addition, this plasma system also provides a bipolar electric field, which could exert polarization assembly effects on the newly formed nanoparticle nuclei.³⁴ The active Cl-rich environment and the assembly effects for the nanoparticles in the plasma bipolar electric field together lead to the self-confinement for the anatase TiO₂ sheet growth, causing more deficiencies in the newly formed crystal lattice and form electron scavengers such as OVs.³⁵⁻³⁷ Thus we believe that the subband with shorter wavelength (subband 1) can be attributed to this lattice defect. Since the sheath region (the space between the two electrodes) of the reactor is only 0.57 mm, other effects of the discharge process such as the ion bombardment to the substrate are almost invisible.

In addition, electron traps were also demonstrated to dominate the emission spectrum of anatase TiO₂ crystals, exhibiting a PL peak at ~650 nm.³¹ Detailed investigation ascribed this red PL to the radiative recombination of trapped electrons, about 0.7-1.6 eV below the conduction band edge with valence band holes. It is not surprised that fitting peaks at similar wavelength (subband 2 in current study) have also been detected in our case, which is especially likely to be caused by the existence of such electron traps. In the discharge process, the TiO₂ crystal growth is accompanied by self-release of ClO in the discharge atmosphere, which has been proved to own the ability to remove oxygen from the stoichiometric TiO₂ due to its special recombination mechanism, and then subsequently introduce uncoordinated Ti atoms (e.g. Ti³⁺) as electron traps without damaging its crystal regularity.³⁸

To further prove the existence of both OVs and Ti³⁺ in our sample, we have carried out XPS analyses (the measured area is 4×6 mm²), and the results are plotted in Fig. 5. In the results of Ti2p (Fig. 5(a)), the peaks of Ti⁴⁺(2p_{3/2}) and Ti⁴⁺(2p_{1/2}) were confirmed with binding energy of 458.3 eV and 464.0 eV, which both have a visible red shift compared with the values from the previous literatures.^{39,40} This phenomena should be mainly attributed to the influence of uncoordinated Ti. It is reported that Ti³⁺ located with lower binding energy will exert strong effect on the symmetric centre of the adjacent Ti⁴⁺ peaks, which will finally lead this variation.^{40,41} Besides, one can easily detect from the XPS spectra that the O1s peak (Fig. 5(b)) suffers

from an asymmetry shape due to the effect of the defects. The peak was fitted and divided into two subbands, which corresponds to Ti^{4+} and Ti^{3+} , separately.⁴⁰ Both of the above features shown in Ti2p and O1s spectra suggested the existence of oxygen vacancy- Ti^{3+} state.⁴²

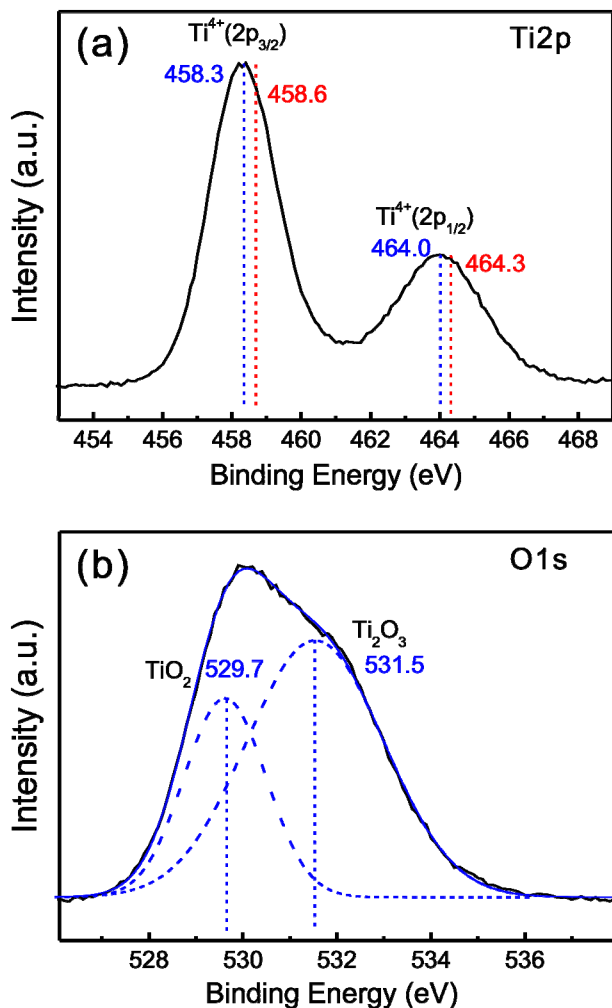


Fig. 5 XPS spectra of the TiO_2 film. (a) Ti2p: Comparisons were made between the standard value (red dashed lines) and measured value (blue dashed lines) in order to clarify the existence of oxygen vacancies and uncoordinated Ti; (b) O1s: The peak of O1s was fitting into two gauss subbands corresponding to Ti^{4+} and Ti^{3+} .

It is worth noting that the integral area and the height ratios of the two subbands are altered at different spots: The subband 1 from OV's becomes stronger around the boundary zone. As discussed above, the film around the boundary zone is deposited at highest temperature and the high temperature disturbs the lattice growth, enhancing the possibility of formation of OV's. Additionally, it should also be pointed out that the high temperature in this area can greatly influence the surface recombination coefficient of O or Cl through reactive release of ClO in our reaction system,³⁷ which will occupy an oxygen lattice site and is also believed as possibility of the enhancement of OV's.³⁸ Since it has been reported that OV's are the most common defect related to lattice plane (101) and in the view of the aforementioned XRD results, the increase of OV's in boundary zone is not strange.⁴³

Conclusions

In summary, anatase TiO_2 films with different morphologies and controllable lattice orientation have been successfully fabricated on quartz substrate in atmospheric pressure by PECVD process. Anatase films obtained in in-glow discharge zone and afterglow discharge zone exhibited various structural properties and were investigated in details with microstructural characterizations, in which visible PL emission is detected for the reason of various lattice defects. The temperature and the ion density in the deposition process are viewed as the main factors which finally determine the lattice structure and the defect properties of obtained anatase films. By changing the deposition parameters in the PECVD system, we should be able to selectively introduce lattice defects and efficiently modify the crystal structure in order to satisfy various demands in the practical applications.

Acknowledgements

This work is supported by the Natural Science Foundation of China (Nos. 51322201 and 51102049), "Shu Guang" project by Shanghai Municipal Education Commission and Shanghai Education Development Foundation, Project Based Personnel Exchange Program with CSC and DAAD, Specialized Research Fund for the Doctoral Program of Higher Education (No. 20120071110025), and Science and Technology Commission of Shanghai Municipality (Nos. 12520706300 and 12PJ1400500).

Notes and references

^a College of Science, Donghua University, Shanghai 201620, China and State Key Laboratory for Modification of Chemical Fibers and Polymer Materials, College of Materials Science and Engineering, Donghua University, Shanghai 201620, People's Republic of China. Email: JShi@dhu.edu.cn

^b Department of Materials Science, Fudan University, Shanghai 200433, People's Republic of China. Email: gshuang@fudan.edu.cn
Electronic Supplementary Information (ESI) available: [Additional SEM and TEM images of the TiO_2 films]. See DOI: 10.1039/b000000x/

- 1 B. Oregan and M. A. Gratzel, *Nature*, 1991, **353**, 737.
- 2 M. Gratzel, *Nature*, 2001, **414**, 338.
- 3 A. Furube, T. Asahi, H. Masuhara, H. Yamashita and M. Anpo, *J. Phys. Chem. B*, 1999, **103**, 3120.
- 4 O. Yamamoto, K. Alvarez, T. Kikuchi and M. Fukuda, *Acta Biomater.*, 1999, **5**, 3605.
- 5 S. Gelover, L. A. Gomez, K. Reyes and M. T. Leal, *Water Res.*, 2006, **40**, 3274.
- 6 U. Diebold, N. Ruzycycki, G. S. Herman and A. Selloni, *Catal. Today*, 2003, **85**, 93.
- 7 J. G. Yu, L. F. Qi and M. Jaroniec, *J. Phys. Chem. C*, 2010, **114**, 13118.
- 8 K. Zhu, N. R. Neale, A. Miedaner and A. J. Frank, *Nano Lett*, 2007, **7**, 69.
- 9 D. Zhang, G. Li, H. Wang, K. M. Chan and J. C. Yu, *Cryst. Growth Des.*, 2010, **10**, 1130.
- 10 M. Lazzeri, A. Vittadini and A. Selloni, *Phys. Rev. B*, 2001, **63**, 155409.
- 11 W. S. Wang, D. H. Wang, W. G. Qu, L. Q. Lu and A. W. Xu, *J. Phys. Chem. C*, 2012, **116**, 19893.
- 12 Z. Zheng, B. Huang, X. Qin, X. Zhang, Y. Dai, M. Jiang, P. Wang and M. H. Whangbo, *Chem.-Eur. J.*, 2009, **15**, 12576.
- 13 H. Wang, J. Gao, T. Guo, R. Wang, L. Guo, Y. Liu and J. Li, *Chem. Commun.*, 2012, **48**, 275.
- 14 J. Miao and B. Liu, *Rsc Adv.*, 2013, **3**, 1222.

- 15 T. R. Gordon, M. Cargnello, T. Paik, F. Mangolini, R. T. Weber, P. Fornasiero and C. B. Murray, *J. Amer. Chem. Soc.*, 2012, **134**, 6751.
- 16 H. G. Yang, C. H. Sun, S. Z. Qiao, J. Zou, G. Liu, S. C. Smith, H. M. Cheng and G. Q. Lu, *Nature*, 2008, **453**, 638.
- 17 T. Ohsawa, M. A. Henderson and S. A. Chambers, *J. Phys. Chem. C*, 2010, **114**, 6595.
- 18 Y. He, O. Dulub, H. Cheng, A. Selloni and U. Diebold, *Phys. Rev. Lett.*, 2009, **102**, 106105.
- 19 H. Yanagi, S. Y. Chen, P. A. Lee, K. W. Nebesny, N. R. Armstrong and A. Fujishima, *J. Phys. Chem.*, 1996, **100**, 5447.
- 20 V. S. Lusvardi, M. A. Barteau, J. G. Chen, J. Eng, B. Fruhberger and A. Teplyakov, *Surf. Sci.*, 1998, **397**, 237.
- 21 A. J. Frank, N. Kopidakis and J. van de Lagemaat, *Coordin. Chem. Rev.*, 2004, **248**, 1165.
- 22 J. Nisar, Z. Topalian, A. De Sarkar, L. Osterlund and R. Ahuja, *ACS Appl. Mater. Interfaces*, 2013, **5**, 8516.
- 23 M. L. Li, G. S. Huang, Y. Q. Qiao, J. Wang, Z. Q. Liu, X. Y. Liu and Y. F. Mei, *Nanotechnology*, 2013, **24**, 305706.
- 24 R. Wang, K. Hashimoto, A. Fujishima, M. Chikuni, E. Kojima, A. Kitamura, M. Shimohigoshi and T. Watanabe, *Adv. Mater.*, 1998, **10**, 135.
- 25 G. M. Wang, H. Y. Wang, Y. C. Ling, Y. C. Tang, X. Y. Yang, R. C. Fitzmorris, C. C. Wang, J. Z. Zhang and Y. Li, *Nano Lett.*, 2011, **11**, 3026.
- 26 D. Zhang, G. Li, X. Yang and J. C. Yu, *Chem. Commun.*, 2009, **29**, 4381.
- 27 S. D. Burnside, V. Shklover, C. Barbe, P. Comte, F. Arendse, K. Brooks and M. Gratzel, *Chem. Mater.*, 1998, **10**, 2419.
- 28 Y. Dai, C. M. Cobley, J. Zeng, Y. Sun and Y. Xia, *Nano Lett.* 2009, **9**, 2455.
- 29 L. Qian, Z. S. Jin, S. Y. Yang, Z. L. Du and X. R. Xu, *Chem. Mater.*, 2005, **17**, 5334.
- 30 G. S. Huang, X. L. Wu, Y. F. Mei, X. F. Shao and G. G. Siu, *J. Appl. Phys.*, 2003, **93**, 582.
- 31 C. C. Mercado, F. J. Knorr, J. L. McHale, S. M. Usmani, A. S. Ichimura and L. V. Saraf, *J. Phys. Chem. C*, 2012, **116**, 10796.
- 32 C. C. Mercado, F. J. Knorr and J. L. McHale, *ACS Nano*, 2012, **6**, 7270.
- 33 C. Lazzaroni, P. Chabert, M. A. Lieberman, A. J. Lichtenberg and A. Leblanc, *Plasma Sources Sci. T.*, 2012, **21**, 035013.
- 34 Q. Y. Yang, D. X. Wang, Y. Guo, K. Ding, J. Z. Xu, J. J. Shi and J. Zhang, *J. Phys. D: Appl. Phys.*, 2011, **44**, 5.
- 35 Z. Zhang and J. T. Yates Jr, *J. Phys. Chem. Lett.*, 2010, **1**, 2185.
- 36 K. Yamada, H. Yamane, S. Matsushima, H. Nakamura, T. Sonoda, S. Miura and K. Kumada, *Thin Solid Films*, 2008, **516**, 7560.
- 37 E. G. Thorsteinsson and J. T. Gudmundsson, *Plasma Sources Sci. T.*, 2010, **19**, 015001.
- 38 E. McCafferty, *Corros. Sci.*, 1995, **37**, 481.
- 39 M. Xing, W. Fang, M. Nasir, Y. Ma, J. Zhang and M. Anpo, *J. Catal.*, 2013, **297**, 236.
- 40 X. Zhang, H. Tian, X. Wang, G. Xue, Z. Tian, J. Zhang, S. Yuan, T. Yu and Z. Zou, *Mater. Lett.*, 2013, **100**, 51.
- 41 F. Guillemot, M. C. Porte, C. Labrugere and C. Baquey, *J. Colloid Interf. Sci.*, 2002, **255**, 75.
- 42 Y. Yu, K. Wu and D. Wang, *Appl. Phys. Lett.*, 2011, **99**, 192104.
- 43 D. J. Kim, S. I. Pyun and Y. G. Yoon, *J. Alloy. Compd.*, 1996, **235**, 182.